Available online at www.sciencedirect.com
SCIENCE DIRECT®
Journal of Magnetic Resonance 165 (2003) 309–314
JMR Journal of Magnetic Resonance
www.elsevier.com/locate/jmr

Communication

Isolating quantum coherences in structural imaging using intermolecular double-quantum coherence MRI

Chih-Liang Chin,[a] Xiaoping Tang,[b,1] Louis-S. Bouchard,[b] Punam K. Saha,[a] Warren S. Warren,[b] and Felix W. Wehrli[a,*]

[a] *Department of Radiology, University of Pennsylvania Medical Center, Philadelphia, PA 19104-4283, USA*
[b] *Department of Chemistry, Princeton University, Princeton, NJ, USA*

Received 22 May 2003; revised 15 August 2003

Abstract

Intermolecular multiple-quantum coherence (iMQC) MR imaging provides a fundamentally different contrast mechanism. It allows probing tissue microstructure by tuning the direction and strength of the correlation gradient. However, iMQC images of a specific quantum-coherence can easily be contaminated by leakage signals from undesired quantum coherences (zero, single, and triple quantum coherence in this work). Using a modified double-quantum CRAZED imaging sequence, we show that signals originating from various coherence orders ($M = 0, 1, 2, 3$) can be predicted in k-space and effectively isolated by means of a four-step phase cycling scheme and judicious choice of flip angles. Finally, preliminary data suggest the method to be able to provide information on trabecular bone architecture such as regional mean trabecular plate separation.

Keywords: Intermolecular multiple-quantum coherence; Trabecular bone; Dipolar field; MRI; Phase cycling

1. Introduction

The signal generated by distant dipolar interactions can be explained as resulting from the mean demagnetizing field which leads to the generation of multiple spin echoes (MSEs) [1,2] or, alternatively, from intermolecular multiple-quantum coherence (iMQC) [3,4]. Recent work has shown that iMQC imaging provides contrast that is fundamentally different from that of conventional MRI techniques [5–8]. The dipolar field giving rise to these effects is caused by distant spins separated by the correlation distance [3,4,9]. Thus, iMQC imaging offers the potential to probe structure size at different scale by tuning the correlation distance. This dipolar field effect has previously been exploited to study structured samples [9–11]. Bowtell et al. reported a Fourier-space formalism describing the relationship between the amplitude of MSE signal and the structure of heterogeneous samples, suggesting that in periodic structures diffraction phenomena might be observed [9,10]. Using a phantom of glass beads, Capuani et al. [11] ascribed the dip in the signal intensity ratio of the second and first echo plotted as a function of the correlation distance to the pore size. Extending CRAZED-type pulse sequences to imaging [8,12,13], the spatial sensitivity of iMQC signals has been recently demonstrated by directly imaging the long-range dipolar field in structured samples [12]. Finally, by varying the direction of the correlation gradient, the method may be able to evaluate structural anisotropy [8].

Here, we investigate the potential of iMQC imaging for probing trabecular bone structure at a spatial resolution that simultaneously permits direct visualization and quantification of trabecular network architecture. In this manner, the observed signal modulations as a function of correlation distance can be compared with actual structural parameters. Unlike in structured phantoms, the structural heterogeneity inherent to trabecular bone is likely to smear out the diffraction-like signal behavior observed in studies of structured

* Corresponding author. Fax: 1-215-349-5925.
E-mail address: wehrli@oasis.rad.upenn.edu (F.W. Wehrli).
[1] Present address: Department of Physics, University of Nevada at Reno, Reno, NV 89557, USA.

1090-7807/$ - see front matter © 2003 Elsevier Inc. All rights reserved.
doi:10.1016/j.jmr.2003.08.007

materials [10,11]. To investigate this effect, iMQC images of bone specimens were acquired to examine the dependence of signal behavior on local trabecular architecture. First, we demonstrate with a modified double-quantum CRAZED imaging sequence [6,14] that the iMQC signals generated from various coherence pathways yield predictable signals in k-space. Second, we show that these signals can be isolated by applying a four-step phase cycling scheme and judicious choice of flip angles, thus providing a means to eliminate imaging artifacts resulting from undesired pathways. Third, we apply this approach to probe trabecular bone architecture. Images acquired at various correlation distances are used to investigate the correlation between signal intensity and mean trabecular separation.

2. Materials and methods

2.1. Sample preparation and MRI experiments

Specimens of the human distal radius harvested previously for a different project were used. Two cylindrical trabecular bone specimens were cored (2.5 cm in diameter and 1.2 cm in thickness) using diamond band saw (Gryphon C-40, Sylmar, CA, USA) and the marrow was removed by immersion in trichloroethylene (Sigma–Aldrich, St. Louis, MO, USA) for 4 h and rinsed with a high-pressure water jet [15]. Finally, the bone samples were wrapped with Parafilm (American Can Company, Greenwich, CT, USA) and placed in saline-filled cylindrical plastic vials for imaging. All experiments were carried out on a 4T GE Signa scanner (GE Medical Systems, Milwaukee, WI, USA) using a home-built solenoidal coil (3.4 cm in diameter). The iMQC MR images were acquired with a modified double-quantum CRAZED pulse sequence shown in Fig. 1. The pulse sequence was validated with bulk measurements on water, in which signal magnitude for a correlation gradient parallel to the B_0 field is twice the value expected when the gradient is perpendicular to the field and negligible at the magic angle [16]. Images of trabecular bone specimens were acquired with the following imaging parameters: TR/TE/τ = 5000/200/30 ms, FOV = 4×4 cm, slice thickness = 2.0 mm, and matrix size = 256×128, while the principal axis of trabecular elements is perpendicular to the B_0 field. RF excitation was accomplished with B_1-insensitive adiabatic pulses [17] of flip angle $\alpha = \pi/2$ (adiabatic half-passage, AHP) and $\beta = \pi/6$ (B_1-insentitive rotation, BIR-4). A four-step phase cycling scheme (Xiaoping Tang et al., unpublished) was applied to the α-pulse, $\phi_\alpha = (x, -x, y, -y)$, while the phase of the β-pulse was held constant, $\phi_\beta = (x)$. In order to isolate signal generated from various coherence transfer pathways, $M = 0$ (ZQC), 1(SQC), 2 (DQC), and 3 (TQC), the data of each excitation was stored and combined by cycling the receive phase (ϕ_{rec}) as indicated in Table 1. Measurements were repeated at various correlation distances (D_c = 200, 500, 800, and 1600 μm) with the correlation gradient applied either perpendicular or parallel to the principal axis of trabecular elements.

2.2. K-space signal analysis for various coherence pathways

IMQC images of a specific M-quantum coherence can be contaminated by undesired coherences, thus complicating interpretation of iMQC contrast and hampering its application to retrieving structural information. The spurious signals can readily be identified since at $k = 0$ (i.e., where the spatial encoding gradients are balanced), a signal resulting from encoding by the correlation gradients may occur. Referring to the pulse sequence of Fig. 1, it becomes clear that for spins evolving with coherence order M during the τ period, the

Table 1
Four-step phase cycling scheme for the coherence order selection

	ZQC	SQC	DQC	TQC
ϕ_α	ϕ_{rec}	ϕ_{rec}	ϕ_{rec}	ϕ_{rec}
x	x	x	x	x
$-x$	x	$-x$	x	$-x$
y	x	$-y$	$-x$	y
$-y$	x	y	$-x$	$-y$

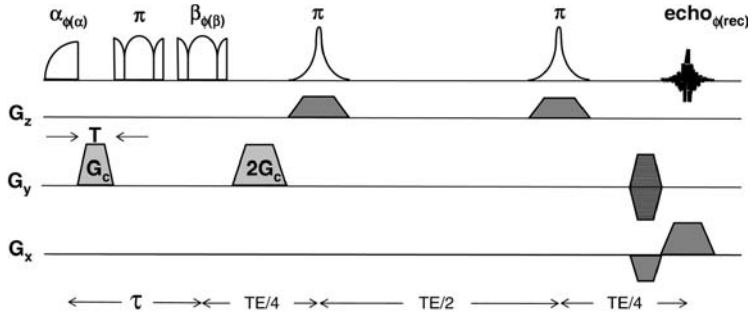

Fig. 1. Modified double-quantum CRAZED imaging sequence: RF pulses of flip angle α (AHP), β (BIR-4), as well as the first π pulse (BIR-4), are adiabatic to achieve uniform excitation and refocusing [17]. Hyperbolic secant refocusing pulses are used for slice-selection.

residual k-value, Δk_c^M, arising from the pair of correlation gradients, can be expressed as

$$\Delta k_c^M = (2-M) \times \frac{\gamma G_c T}{2\pi} = \frac{(2-M)}{2D_c}, \quad (1)$$

where G_c is the amplitude of the correlation gradient immediately following the α-pulse and $D_c = \pi/(\gamma G_c T)$. The maximum values of k_x and k_y in 2D k-space are given as

$$k_{x,y}^{MAX} = \frac{N_{x,y}}{2FOV_{x,y}}, \quad (2)$$

where $FOV_{x,y}$ and $N_{x,y}$ are the field-of-view and the number of encoding steps along either x or y direction. When $\Delta k_c^M \leqslant k_{x,y}^{MAX}$, the phase of the spurious signals will be unwound by the spatial encoding gradients; thus leading to refocusing at a location shifted with respect to the center of k-space by $\Delta n_{x,y}^M$ pixels

$$\Delta n_{x,y}^M = \frac{\Delta k_c^M}{k_{x,y}^{MAX}} \times \frac{N_{x,y}}{2} = (2-M) \times \frac{FOV_{x,y}}{2D_c}. \quad (3)$$

The situation is different when the correlation gradient is parallel to the slice-selection gradient. In this case, the unwanted coherences imbalance the slice selection gradient and thus will not be re-phased.

3. Results and discussion

3.1. Spurious k-space signals

Fig. 2 shows the k-space data of iDQC images obtained with different phase cycling schemes. Significant contamination by spurious signals is observed without phase cycling (Fig. 2a). It is noted that artifactual signal maxima appear at $k_y = \Delta k_c^M$. According to Eq. (3), the pixel offset $\Delta \mathbf{n}_Y$ of these artifactual signals is 50 ($M = 0$), 25 ($M = 1$), and −25 ($M = 3$). Notably, the appearance of a TQC signal is surprising, given that its intensity is at least two orders of magnitude lower than its SQC counterpart [18]. Two-step phase cycling virtually removes the strong SQC signal (Fig. 2b) whereas the ZQC signal survives. As one would predict, the leakage signals cause modulations in image space, which lead to banding artifacts (Fig. 2c). This observation explains the residual modulations described by Bouchard et al. [13], in which only a two-step phase cycling has been used for iDQC imaging. However, the DQC signal can effectively be isolated through use of a four-step phase cycling (Fig 2d). Although four-step phase cycling is unable to remove unwanted signals generated by higher-order coherence pathways ($M > 3$), our results indicate the four-step phase cycling to be sufficient in light of the low intensity of higher coherence-order signals. Alternatively, coherence order selection can be achieved by a four-step phase cycling scheme in which all quadrature combinations of α and β pulses are used, as described by Minot et al. [18]. In addition, the selected small flip angle of the β-pulse also facilitates suppressing unwanted signals (all minus quantum coherences).

As expected, the banding artifacts disappear in the reconstructed image if the correlation gradient is applied along slice-selection direction (Fig. 2f), although the signal intensity is decreased by a factor of two due to its dipolar angle dependence. Nevertheless, four-step phase

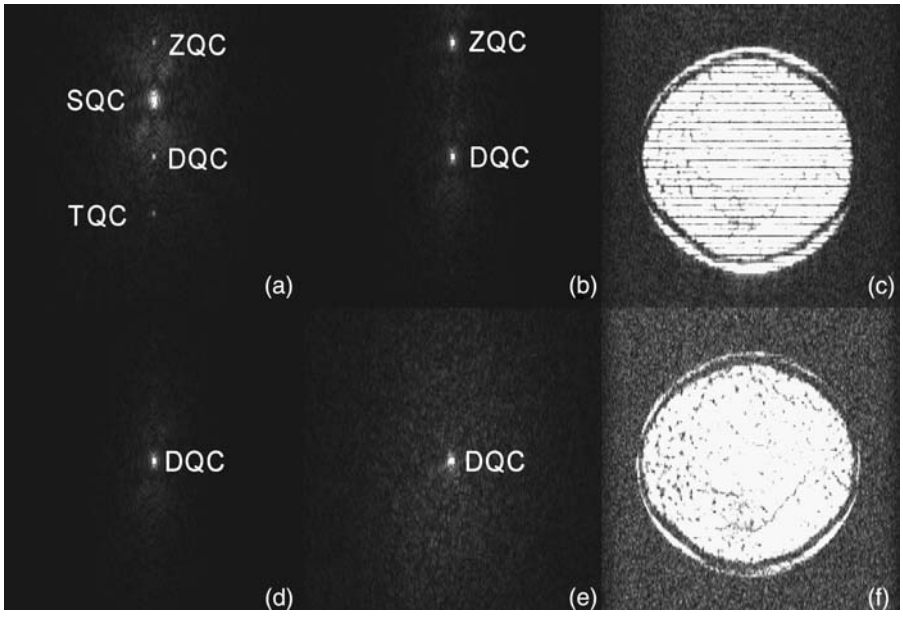

Fig. 2. Averaged iMQC k-space data and images of trabecular bone sample for different phase cycling schemes ($D_c = 800\,\mu m$): non-phase-cycled (a), two-step phase-cycled (b) and the corresponding image (c), four-step phase-cycled (d). The two-step phase-cycled image shows significant modulations caused by ZQC signal contamination. When the correlation gradient is applied along the slice-select direction, no spurious echo is observed (e, non-phase-cycled) and the image reconstructed does not present a banding artifact (f, two-step phase-cycled).

cycling should further improve coherence order selectivity. Previous iMQC imaging experiments were often performed with the correlation gradient applied along the slice selection direction to avoid its possible interference with spatial encoding gradients [6,13,19]. Since the correlation gradient for an unwanted coherence pathway imparts a magnetization helix which translates into a phase modulation across pixels. Thus, the unwanted signal should vanish as long as the correlation distance is much less than the pixel size. However, in some circumstances, the spurious signal might persist. Possible situations include a non-integer number of helix cycles per pixel, an inhomogeneous distribution of spin density (as one might expect, for example, for trabecular bone), or the intervention of strong local field gradients. Therefore, four-step phase cycling is important in applications of iMQC imaging to the study of quasi-regular heterogeneous structures such as trabecular bone networks which are inherently anisotropic and thus require measurement at more than one orientation of the correlation gradient.

3.2. Assessment of trabecular architecture

The iDQC images of bone specimens acquired at various correlation distances are shown in Figs. 3b–e. It is noted that the image contrast is a function of correlation distance, a behavior that depends on local trabecular architecture, while an edge attenuation effect is observed at the largest correlation distance [12]. Similarly, signal loss occurs at the boundary between bone and water, causing the trabecular elements to appear thicker than in the SQC image (Fig. 3a). This observation is consistent with prior

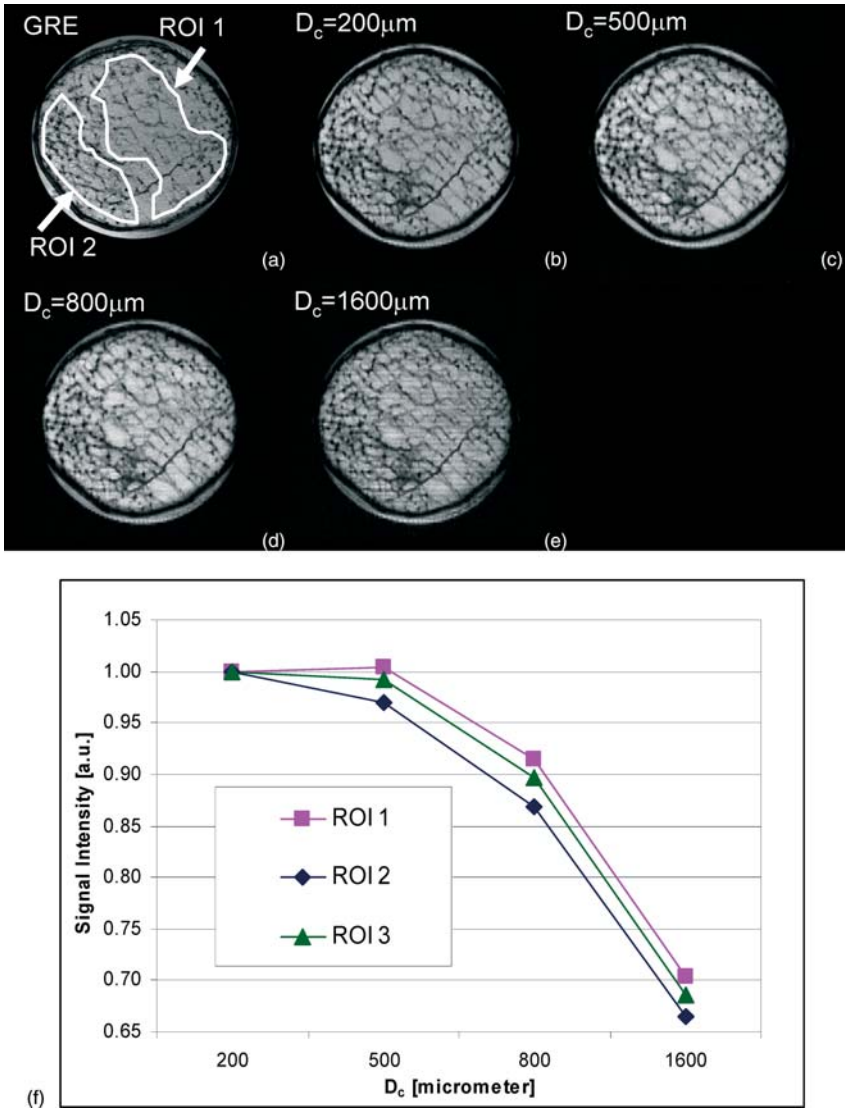

Fig. 3. A gradient-echo reference image (pixel size = $156 \times 156\ \mu m^2$) of the trabecular bone specimen (a); IDQC images of trabecular bone acquired at various correlation distances (b–e); plot of iDQC signal intensity versus correlation distance for the ROIs indicated in (a) (f); as well as for the average from the entire section (labeled ROI 3). The weak modulations observed in (e) are caused by leakage signals at the large correlation distance selected.

work by Bouchard et al. [13] in a study of structured phantoms. For the modified CRAZED sequence, image intensity is determined by the density of paired spins separated by the correlation distance. Therefore, the signal intensity is expected to increase as the correlation distance approaches the mean trabecular spacing. Consequently, when recording the signal by stepping the correlation distance, trabecular separation (mean distance between trabeculae) can, in principle, be retrieved as preliminary data obtained in capillary arrays suggest [20]. Evidence for such behavior is provided by plots of signal intensity versus correlation distance in two distinctly different regions of interest (ROI) (Fig. 3a). The curve corresponding to ROI 1 suggests a maximum around $D_c = 500\,\mu m$, not seen for corresponding data from ROI 2 (Fig. 3f). To examine the relationship of these findings with actual structural measures, trabecular separation distributions were calculated from the reference image (Fig. 3a) using the fuzzy distance transform method [21]. The mean and standard deviation of these distributions are 675 and 422 μm for the ROI 1 and 467 and 226 μm for ROI 2. These preliminary results suggest that quantitative regional trabecular separation measurements may be possible, although the relatively coarse sampling of correlation distance does not permit quantitative measurements at this stage. It is noted that when the signal from the entire cross-section of the specimen is plotted, a curve intermediate between those from the two ROIs is obtained, reflecting structural heterogeneity (mean/SD = 641/406 μm), suggesting the need for performing localized measurements.

Capuani et al. [11] reported trabecular pore size in bovine femoral bone on the basis of MSE bulk signals. The observed multiple dips, which they claim to occur at values of the correlation distance matching mean trabecular pore size. However, very recent data obtained from bulk measurements (i.e., non-spatially resolved) indicate that such dips are likely the result of performing the experiments without phase cycling [22]. Also, in the work of [11] the retrieved pore sizes were not validated against actual structural measurements. Our preliminary results emphasize the need for localized measurements since trabecular architecture can be highly heterogeneous [23]. Finally, an alternative approach to measure the spatial periodicity of quasi-regular structures is q-space imaging [24,25], for example, to retrieve structural information of biological tissues. However, the typical length scale in that method is on the order of the diffusion distance (i.e., 1–10 μm) whereas trabecular separation is at least two orders of magnitude larger.

4. Conclusions

This work shows that in double-quantum coherence imaging involving dipolar coupling between distant spins, leakage signals from undesired coherence pathways (ZQC, SQC, and TQC) can be eliminated by means of four-step phase cycling and judicious choice of flip angles. Experimental data on trabecular bone specimens suggest the feasibility of retrieving structural parameters such as mean trabecular separation.

Acknowledgments

This research was supported by NSF Grant MRSEC DMR-0213706 and NIH grant CA88683.

References

[1] G. Deville, M. Bernier, J.M. Delrieux, NMR multiple echoes observed in solid ^{3}He, Phys. Rev. B (1979) 5666.
[2] R. Bowtell, R.M. Bowley, P. Glover, Multiple spin echoes in liquids in a high magnetic field, J. Magn. Reson. 88 (1990) 643–651.
[3] W.S. Warren, W. Richter, A.H. Andreotti, B.T. Farmer 2nd, Generation of impossible cross-peaks between bulk water and biomolecules in solution NMR, Science 262 (1993) 2005–2009.
[4] W. Richter, S. Lee, W.S. Warren, Q. He, Imaging with intermolecular multiple-quantum coherences in solution nuclear magnetic resonance, Science 267 (1995) 654–657.
[5] W.S. Warren, S. Ahn, M. Mescher, M. Garwood, K. Ugurbil, W. Richter, R.R. Rizi, J. Hopkins, J.S. Leigh, MR imaging contrast enhancement based on intermolecular zero quantum coherences, Science 281 (1998) 247–251.
[6] J. Zhong, Z. Chen, E. Kwok, New image contrast mechanisms in intermolecular double-quantum coherence human MR imaging, J. Magn. Reson. Imaging 12 (2000) 311–320.
[7] R.R. Rizi, S. Ahn, D.C. Alsop, S. Garrett-Roe, M. Mescher, W. Richter, M.D. Schnall, J.S. Leigh, W.S. Warren, Intermolecular zero-quantum coherence imaging of the human brain, Magn. Reson. Med. 43 (2000) 627–632.
[8] S. Capuani, G. Hagberg, F. Fasano, I. Indovina, A. Castriota-Scanderbeg, B. Maraviglia, In vivo multiple spin echoes imaging of trabecular bone on a clinical 1.5 T MR scanner, Magn. Reson. Imaging 20 (2002) 623–629.
[9] R. Bowtell, P. Robyr, Structural Investigations with dipolar demagnetizing field in solutions NMR, Phys. Rev. Lett. 76 (1996) 4971–4974.
[10] P. Robyr, R. Bowtell, Nuclear magnetic resonance microscopy in liquids using the dipolar field, J. Chem. Phys. 106 (1997) 467–476.
[11] S. Capuani, F. Curzi, F.M. Alessandri, B. Maraviglia, A. Bifone, Characterization of trabecular bone by dipolar demagnetizing field MRI, Magn. Reson. Med. 46 (2001) 683–689.
[12] R. Bowtell, S. Gutteridge, C. Ramanathan, Imaging the long-range dipolar field in structured liquid state samples, J. Magn. Reson. 150 (2001) 147–155.
[13] L.S. Bouchard, R.R. Rizi, W.S. Warren, Magnetization structure contrast based on intermolecular multiple-quantum coherences, Magn. Reson. Med. 48 (2002) 973–979.
[14] S. Garrett-Roe, W.S. Warren, Numerical studies of intermolecular multiple quantum coherences: high-resolution NMR in inhomogeneous fields and contrast enhancement in MRI, J. Magn. Reson. 146 (2000) 1–13.
[15] D.J. Sharp, K.E. Tanner, W. Bonfield, Measurement of the density of trabecular bone, J. Biomech. 23 (1990) 853–857.
[16] W. Richter, M. Richter, W.S. Warren, H. Merkle, P. Andersen, G. Adriany, K. Ugurbil, Functional magnetic resonance imaging

with intermolecular multiple-quantum coherences, Magn. Reson. Imaging 18 (2000) 489–494.
[17] M. Garwood, L. DelaBarre, The return of the frequency sweep: designing adiabatic pulses for contemporary NMR, J. Magn. Reson. 153 (2001) 155–177.
[18] E.D. Minot, P.T. Callaghan, N. Kaplan, Multiple echoes, multiple quantum coherence, and the dipolar field: demonstrating the significance of higher order terms in the equilibrium density matrix, J. Magn. Reson. 140 (1999) 200–205.
[19] J.P. Marques, S. Gutteridge, R. Bowtell, Optimising the signal to noise ration in double quantum CRAZED imaging, Proc. Int. Soc. Magn. Res. Med., Tenth Scientific Meeting, Honolulu, Hawaii, USA: ISMRM 2287, 2002.
[20] C.L. Chin, X. Tang, L.S. Bouchard, W.S. Warren, F.W. Wehrli, NMR diffraction revisited with a modified CRAZED double quantum imaging sequence, Proc. Int. Soc. Magn. Res. Med., Eleventh Scientific Meeting, Toronto, Ontario, Canada: ISMRM 803, 2003.
[21] P.K. Saha, F.W. Wehrli, B.R. Gomberg, Fuzzy distance transform: theory, algorithms, and applications, Comput. Vision Image Understanding 86 (2002) 171–190.
[22] L.S. Bouchard, C.L. Chin, X. Tang, W.S. Warren, F.W. Wehrli, Structural characterization of trabecular bone using bulk NMR measurements of intermolecular multiple-quantum coherence, Proc. Int. Soc. Magn. Res. Med., Eleventh Scientific Meeting, Toronto, Ontario, Canada: ISMRM 1113, 2003.
[23] B.R. Gomberg, P.K. Saha, F.W. Wehrli, Topology-based orientation analysis of trabecular bone networks, Med. Phys. 30 (2003) 158–168.
[24] P.T. Callaghan, Principles of Nuclear Magnetic Resonance Microscopy, Oxford University Press, Oxford, 1993.
[25] D.G. Cory, A.N. Garroway, Measurement of translational displacement probabilities by NMR: an indicator of compartmentation, Magn. Reson. Med. 14 (1990) 435–444.